IOP Publishing Measurement Science and Technology
Meas. Sci. Technol. **31** (2020) 085106 (11pp) https://doi.org/10.1088/1361-6501/ab82c0

3D image reconstruction using an ECT sensor with a single layer of electrodes

Jingjing Shen[1,2], Shuanghe Meng[1], Mao Ye[1], Wuqiang Yang[3] and Zhongmin Liu[1]

[1] Dalian National Laboratory for Clean Energy and National Engineering Laboratory for MTO, Dalian Institute of Chemical Physics, Chinese Academy of Sciences, Dalian 116023, People's Republic of China
[2] University of Chinese Academy of Sciences, Beijing 100049, People's Republic of China
[3] Department of Electrical and Electronic Engineering, The University of Manchester, Manchester M13 9PL, United Kingdom

E-mail: maoye@dicp.ac.cn

Received 14 December 2019, revised 17 March 2020
Accepted for publication 24 March 2020
Published 26 May 2020

Abstract

Sensor design is important for electrical capacitance tomography (ECT) that is to be used for a particular application and for generating high-quality images from the measured data. An ECT sensor with long electrodes is commonly used to obtain stable and reliable measurement signals and to ensure the quality of 2D cross-sectional images, but it neglects the effect of electrode length on the entire 3D image. To analyze the effect of electrode length on the measured signals, sensitivity distribution and the quality of reconstructed images, especially the distortion of 3D images, ECT sensors with different electrode lengths of 5, 7, 10, 20 and 30 mm are designed and fabricated. The electrodes are mounted on the internal surface of the ECT sensor wall to eliminate the negative effect of the wall. A dual-electrode excitation strategy is chosen to enhance the signal intensity. The results show that the reconstructed 3D images of the measured objects, which can be divided into three parts, are stretched in the axial direction and narrowed in the radial direction because of the axial average effect, and longer electrodes result in a more serious problem. Comprehensive analysis of the performance of the ECT sensors with different electrode lengths, including the measured signals, sensitivity distribution and reconstructed 3D images, concludes that an ECT sensor with an electrode length of 10 mm is recommended.

Keywords: 3D image, electrode length, axial average effect, ECT

(Some figures may appear in colour only in the online journal)

1. Introduction

Electrical capacitance tomography (ECT) has been widely considered as a robust and economic approach for visualizing the material distribution inside a closed space supposing that the permittivity of the material of interest differs significantly from that of the surrounding media. The applications of ECT can be found in either imaging solid objects [1–3] or visualizing the two-phase processes [4–6].

Most of the time, the 2D cross-sectional images by ECT cannot provide sufficient information as the objects in the real world are 3D. For instance, we cannot obtain the real shape and volume of the object as a circle in 2D ECT images might represent a cylinder, a cone or a sphere with a circular cross section. Therefore, obtaining 3D ECT images of objects is highly desired. The most direct way to get a 3D ECT image is to use an ECT sensor with multi-layer electrodes [7]. However, it has long been a big challenge to directly reconstruct 3D images using a multi-layer ECT sensor. A multi-layer ECT sensor normally has multi-layer electrodes and needs more electrodes to achieve the required sufficient spatial resolution of the reconstructed 3D images, which makes the design and fabrication of the corresponding hardware extremely complicated and expensive, if not impossible [8]. On one hand, the measuring signal between a pair of electrodes at different layers is much weaker than that between a pair of electrodes at the same layer, which leads to a relatively high signal-to-noise ratio [9]. On the other hand, the optimal design of the sensor, especially regarding the electrode number [10],

electrode length [11], number of layers [7] and angular distribution of electrodes [12], is yet to be further understood and remains a non-trivial task.

Meanwhile, the scheme and design of an ECT sensor with single-layer electrodes are well established. Therefore, it has become common practice in ECT measurement to obtain 3D images by interpolating 2D images obtained in a consecutive time series [13–16]. Liu *et al* used elementary iso-surfaces to make smooth connections of continuous 2D images on the basis of stacking [17]. The design of the sensor is considered firstly, and to avoid the fringe effect and give sufficiently large capacitance, long electrodes are commonly used to obtain more stable and reliable measurement signals, usually 10 cm or longer [8], which is to ensure the quality of 2D cross-sectional images and neglects the effect on the reconstruction of 3D ECT images. For an ECT sensor with single-layer electrodes, it is generally assumed that the sensitivity distribution is uniformly distributed along the axial direction in the sensing region, and thus the measured permittivity represents the axial average and is inconsistent with the real measurement conditions, e.g. a fluidized bed. Huang *et al* [18] studied ECT sensors with three different electrode lengths (45, 55 and 65 mm), and they found that bubble diameter decreases with the increase in the electrode length of fluidized beds under the same operational conditions. In real measurement the permittivity between any given pair of electrodes demonstrates a complicated distribution along the axial direction, dependent upon the object in the sensing region, and the axial average effect is more serious [4, 19], but the specific effect is unknown. In this connection, the electrode length, which essentially defines the sensing region, plays a critical role in the reconstruction of 3D ECT images based on 2D images obtained via an ECT sensor with a single-layer electrode. So far, the axial average effect, i.e. the effect of electrode length on image quality, especially for 3D imaging, has not been systematically studied.

Previous results in the literature suggested that an ECT sensor with longer electrodes should be chosen because of the high signal-to-noise ratio. However, the reconstructed 3D images of objects are normally stretched in the axial direction and contracted in the radial direction because of the axial average effect if longer electrodes are used. Therefore, the aim of this work is to investigate the effect of the electrode length of an ECT sensor with single-layer electrodes on the reconstruction of 3D ECT images, especially the distortion of 3D images.

2. Principle of ECT

The first step of reconstructing 3D images of an object is to obtain the 2D cross-sectional images in a consecutive time series by an ECT system, which consists of three parts: (1) a multi-electrode capacitance sensor surrounding a pipe or vessel, (2) sensing electronics and (3) a computer for system control and image reconstruction. First, an ECT sensor converts the permittivity distribution into electrical signals. The number of electrodes in an ECT sensor N_e can be 8, 12 or more, and an excitation electrode i and a detection electrode j form a capacitor. Because of the geometry between the excitation electrode and the detection electrode, the electric field distribution is complicated, causing non-linearity of the measurement. Because of the nature of soft-field sensing, the sensitivity at the edge is higher than that in the center [20, 21]. If there are only two materials with significantly different permittivity in the measurement region, they can be distinguished. When the measurement region is completely filled with low-permittivity material, the measured signals are used for lower-permittivity calibration. Similarly, higher-permittivity calibration is implemented using high-permittivity material [8]. Basically, if the diameter of the ECT sensor is fixed, increasing the number of electrodes will lead to a reduction of the effective sensing area and thus the decrease in the magnitude of the measured capacitance signal for a single pair of electrodes. In addition, the measured signal between a pair of opposite electrodes is much smaller than that between a pair of adjacent electrodes in an ECT sensor. Meanwhile, there exists a low limit of capacitance that can be detected due to the noise and stability of ECT signal processing electronics. In this connection, the number of electrodes of an ECT sensor is restricted by the minimum capacitance that the ECT signal processing electronics can detect. More pixels are needed to obtain high-quality cross-sectional images. Usually, the number of pixels M is far more than that of the independent capacitance measurements N, which causes the ill-posedness of the inverse problem [22].

The capacitance signals are processed by the sensing electronics with amplification, phase-sensitive demodulation, low-pass filtering and so on. Because the capacitance of opposite electrodes in an ECT sensor is only a few femtoFarad (fF), the capacitance measuring circuit used must be sufficiently sensitive, and the surrounding noise and screened cables may have an adverse effect on the measured signals [23, 24]. Therefore, high stability and reliability are needed for ECT measurement. Yang *et al* [25, 26] introduced an AC-based capacitance measuring circuit to deal with those problems.

The measured signals processed by the sensing electronics are sent to a computer to reconstruct the permittivity distribution, and to obtain the dynamic parameters of a process, such as a fluidized bed. The algorithms can be categorized into two groups: (1) single-step algorithms, and (2) iterative algorithms [27]. Linear back projection (LBP) [28] and Tikhonov regularization [29] are commonly used single-step algorithms with short computation time and give qualitative descriptions of a real flow. LBP is often used for on-line monitoring. Iterative algorithms like Landweber iteration can provide good quality images by additional calculation, but more time is needed. Therefore, this method is mainly used for off-line data analysis [30]. The reconstructed permittivity distribution needs further processing (e.g. threshold segmentation) to provide more detailed information on a fluidized bed, such as flow regime identification, solids concentration, the size, and frequency of bubbles[24, 31–33].

The final step is to obtain a 3D image by interpolating 2D ECT images. To maintain a better spatial resolution of 3D images, it needs enough 2D images in the consecutive measurement time series. Note that the measured capacitance signals are normally very weak, and a balance

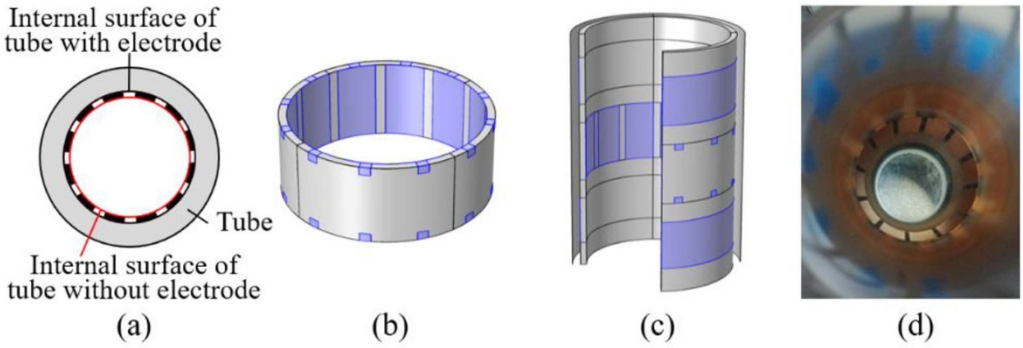

Figure 1. The ECT sensor with internal electrodes: (a) internal electrode, (b) electrode layer, (c) whole sensor, (d) a photograph.

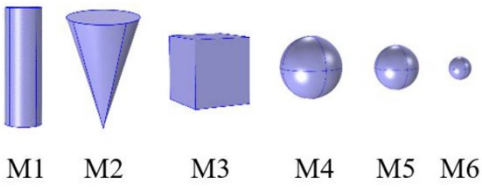

Figure 2. Models used to reconstruct 3D images: (M1) cylinder, $D = 20$ mm, $L = 60$ mm; (M2) cone, $D = 30$ mm, $L = 60$ mm; (M3) cube, $L = 30$ mm; (M4) sphere, $D = 30$ mm; (M5) sphere, $D = 20$ mm; and (M6) sphere, $D = 10$ mm.

between sampling frequency and measurement stability is highly desired. Higher sampling frequency will result in worse stability of the measured signal and vice versa, which relies on the performance of the sensing electronics. For objects moving with a relatively low speed, stable and high-quality 2D ECT images can be readily obtained at a low sampling frequency, which in principle can be further interpolated into 3D ECT images by simply stacking all the 2D images in the order of the time series. For objects moving at a fast speed, complex post-processing, such as the de-noising method [24], is required after interpolation of the 2D images in a consecutive time series.

Figure 3. The automatic control system used for controlling movement of sensors and measured models in the ECT system.

3. Experiment setup

3.1. Sensor design

Figure 1 shows the design of the ECT sensors. Note that the presence of a wall causes extra capacitance [8], which might cause systematical errors to the measuring signals, and also affects the sensitivity. Thus, the electrodes of the ECT sensors are mounted on the internal surface of a quartz glass to eliminate such effects. The electrode lengths are 5, 7, 10, 20 and 30 mm, respectively, with the electrode covering ratio of 80%. If the electrodes of the ECT sensor were directly mounted on the internal surface of the tube, the thickness of the electrodes, if not negligible, would also influence the sensitivity and induce uncertainty to the measurements. Therefore, we first made some channels on the internal surface of the tube by strictly following the arrangement of the electrodes. The width and thickness of the channels were set to properly fit the electrodes, and thus the electrodes could be mounted in the channels to keep the internal surface of the tube as smooth as possible, as shown in figure 1(a), and the inner diameter of the tube was 60 mm. In consideration of the spatial resolution and measurement requirements, 12 electrodes are used in each ECT sensor.

To verify the performance of the ECT sensors, some static models, as shown in figure 2, are fabricated and measured to reconstruct 3D images by stacking consecutive 2D images. Because most bubbles in fluidized beds are approximately spherical, some spheres with different diameters are selected. For the models of known geometric shapes, the quality of the reconstructed images is analyzed to evaluate the performance of the ECT sensors. Because the velocity of gas or the solid phase has a great effect on the reconstructed images, the movement velocity of the models is chosen as 1, 10, 100,

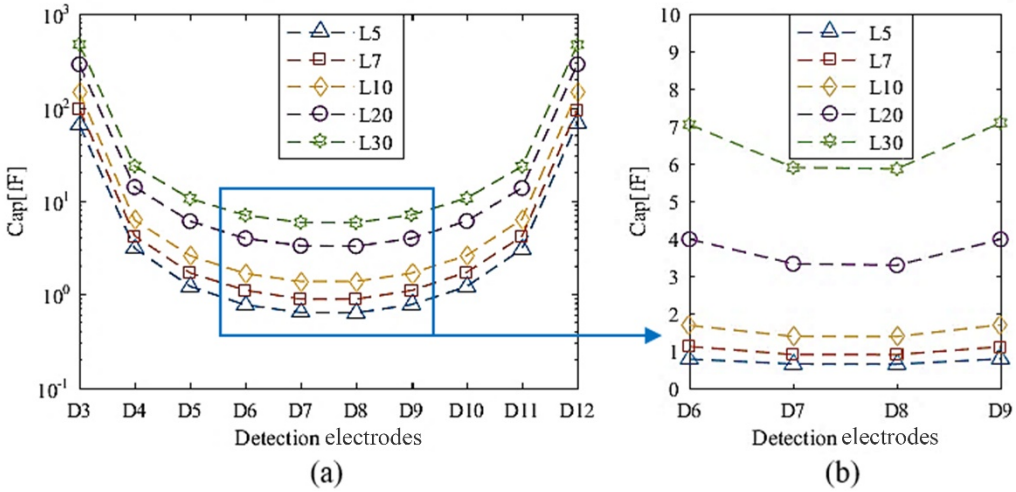

Figure 4. Capacitance data of ECT sensors with different electrode lengths in the axial direction obtained by numerical simulation, when electrodes 1 and 2 are used for excitation and others for detection: (a) when the ECT sensors are filled with low-permittivity materials; (b) the dynamic range when the ECT sensors are filled with high- and low-permittivity materials.

200 and 300 mm s^{-1}. In addition, dual-electrode excitation is chosen to enhance the signal intensity and improve the signal quality.

3.2. Experiment setup

The sensing electronics of the ECT system used are based on an AC-based circuit, as mentioned earlier. To achieve accurate movement velocity of the measured models, an automatic control system was built. It is a closed-loop system, mainly including a control panel, programmable logic controller (PLC), servo driver, servo motor and ball screw, as shown in figure 3. The relative position in the tangential direction of an ECT sensor and the measured model can be turned with a hand-operated screw, bolts and nuts. The main control parameters of this system are the starting/ending position and movement velocity in the axial direction, with precise parameter control and display.

3.3. Image reconstruction

Landweber iteration (equation (1)) is adopted for image reconstruction. The initial image is calculated by LBP (equation (2)). The 2D cross-sectional images are reconstructed from the measured capacitance signals, and then stacked to 3D images of the measured objects:

$$\hat{g}_{k+1} = P\left[\hat{g}_k - \alpha S^T(S\hat{g}_k - \lambda)\right]$$
$$P[f(x)] = \begin{cases} 0 & if \quad f(x) < 0 \\ f(x) & if \quad 0 \le f(x) \le 1 \\ 1 & if \quad f(x) > 1 \end{cases} \tag{1}$$

$$\hat{g}_0 = \frac{S^T\lambda}{S^T u_\lambda} \qquad u_\lambda = [1, 1, \ldots, 1] \ . \tag{2}$$

4. Results and discussion

4.1. Measured signals

Figure 4 shows the measured capacitance data under the conditions of noise-free by finite element numerical simulation when the ECT sensors are filled with low-permittivity material, and the dynamic range of the capacitance data when the ECT sensors are filled with high- and low-permittivity materials. The number in the legend in figure 4 denotes the electrode length of the ECT sensor, e.g. L5 means the length of the ECT sensor is 5 mm. Figure 4 only shows the capacitance data when electrodes 1 and 2 are used for excitation and others for detection for simplification. The data are similar to each other when other electrodes are used for excitation because all the electrodes have the same geometric shape and are distributed evenly.

The capacitance decreases with the increase in the distance between the excitation and detection electrodes when the ECT sensor is filled with low- or high-permittivity materials. The adjacent electrode pairs give the maximum capacitance, and the opposite electrode pairs give the minimum capacitance. The relative position of the excitation and detection electrodes has a great effect on the capacitance. The measurement range of the ECT sensor of L30 is from 5.8 fF to 823 fF, and L5 is from 0.63 fF to 128 fF. The measurement range becomes significantly smaller by removing the maximum capacitance data between the adjacent electrodes, because the maximum capacitance is about one order of magnitude larger than others.

The capacitance in the same relative position of the excitation and detection electrodes is proportional to the electrode length of the ECT sensors approximately. With the decrease in electrode length, it becomes difficult to measure the capacitance because of the decrease in the measured signal intensity. Besides, the fringe effect also becomes more serious.

The ECT sensors were fabricated and experiments were conducted to verify the performance of the ECT sensors with

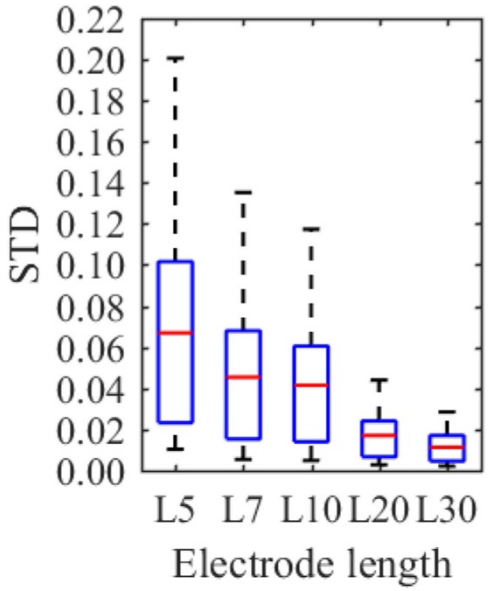

Figure 5. The STD of the measured signals when the ECT sensors are filled with low-permittivity material.

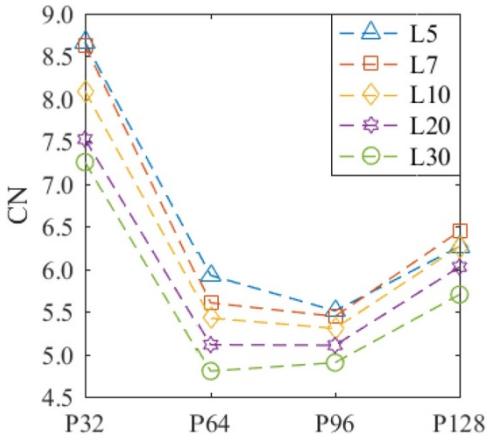

Figure 6. The CN of the sensitivity matrix of the ECT sensor with different electrode lengths when choosing different pixels in the sensing region.

different electrode lengths. There are 120 normalized measured capacitance signals in each frame data in total, and 1000 frames were sampled when an ECT sensor was filled with low-permittivity material, or air. The standard deviation (STD) is used for analyzing the measured signals, as shown in figure 5.

With the decrease in the electrode length of the ECT sensors, the measured signal becomes worse and the measurement stability gradually reduces. The trend of the STD of the measured signals with different electrode lengths agrees with the numerical simulation. When the ECT sensors are filled with low-permittivity material, the normalized capacitance signal fluctuates around 0, which changes considerably for little disturbance, resulting in a large STD. The quality of the measured signals is improved significantly when high-permittivity materials occupied more than 10% of the measuring region [34].

4.2. Sensitivity distribution

The cross-sectional area of the sensing region is always divided into $N_p \times N_p$ pixels, and in this work we took $N_p = 32$, 64, 96 and 128 (denoted by P32, P64, P96 and P128 for simplification) to analyze the sensitivity matrix and optimize the number of pixels for the reconstruction of 3D ECT images. Figure 6 shows the condition number (CN) of the sensitivity matrix for different electrode lengths. As can be seen, with the increase in the number of pixels, the CN of the sensitivity matrix first decreases and then increases, showing a minimum at a certain number of pixels. Note that the CN represents the ill-posedness of the inverse problem in the reconstruction of ECT images, and a higher CN reflects the fact that variation in the measurement signal has a much more severe impact on the quality of the reconstructed ECT images. In this sense, we can conclude that a small number of pixels (e.g. P32) will lead to a low spatial resolution and high CN, both unfavorable to the quality of the reconstructed images. For a large number of pixels (e.g. P128), although the spatial resolution is high, it also results in a high CN. Therefore, P64 and P96 are better choices when compared with P32 and P128 in terms of both spatial resolution and CN.

Figure 7 shows the reconstructed 3D images of M1 using sensor L10 when different numbers of pixels were chosen. With the increase in the number of pixels in the sensing region, the edge blurring of the reconstructed images becomes worse, and the image quality degrades sharply, as seen in figure 7. In this regard, a smaller number of pixels is desired to minimize the blurred edges problem in ECT image reconstruction. But a small number of pixels results in low spatial resolution of the ECT and a high CN, as shown in figure 6. It is generally accepted that the measurement resolution of ECT is restricted by the limited number of independent capacitance and electrodes, which, however, is not evidently added with the increase in the number of pixels in the current case. Therefore, P64 is chosen by comparison of the CN and the edge blurring problem of the reconstructed images with other counterparts, as it can provide relatively high quality of the reconstructed 3D image and a low CN.

The sensitivity varies greatly in different locations of the sensing region of an ECT sensor. Figure 8(a) shows the 3D sensitivity distribution of the ECT sensor L30 choosing the cross-sectional center at the bottom of the tube with electrodes as the origin (0,0,0) when electrodes 1 and 2 are used for excitation and electrode 6 for detection. The sensitivity in the region between the excitation and detection electrodes is remarkably higher than other regions, especially near the excitation and detection electrodes. In addition, it has almost the same sensitivity distribution for voxels in different axial positions (z-coordinate) but the same radial position (x- and y-coordinates), which makes it difficult to reconstruct 3D images directly for the ECT sensors with a single layer of electrodes. The sensitivity distributions of the ECT sensors are analyzed in terms of the STD and CN, as shown in figure 8(b). Comparing the STD of the sensitivity, the homogeneity of the sensitivity first increases and then decreases with the decrease in

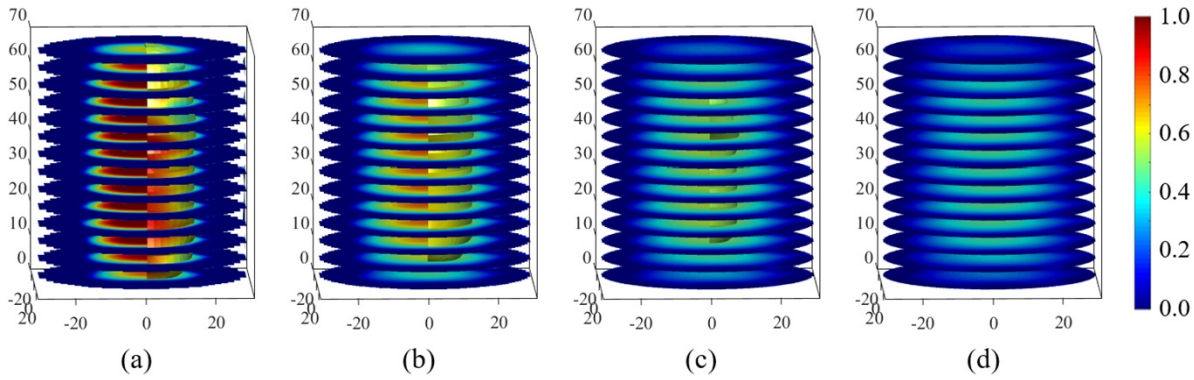

Figure 7. The reconstructed 3D images of M1 using sensor L10 when choosing different numbers of pixels in the sensing region: (a) P32, (b) P64, (c) P96, (d) P128.

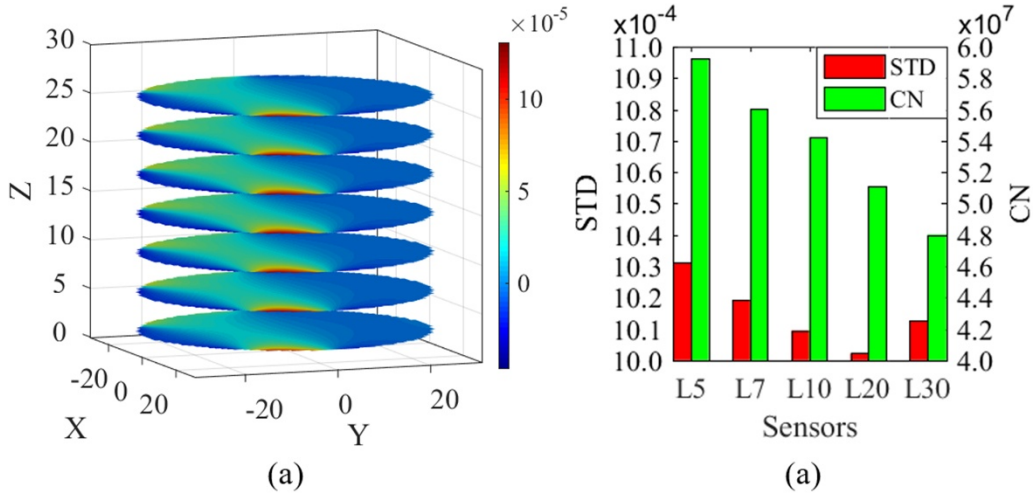

Figure 8. Analysis of the sensitivity distribution: (a) 3D normalized sensitivity distribution of the ECT sensor L30 when electrodes 1 and 2 are used for excitation and electrode 6 for detection. (b) Comparison of the sensitivity fields of ECT sensors with different electrode lengths.

electrode length. The ECT sensors L10 and L20 perform better than the ECT sensor L30 in terms of the STD. The CN increases with the decrease in the electrode length.

4.3. Image reconstruction

Figure 9 shows the reconstructed images by the ECT sensors with different electrode lengths when the movement velocity of the measured model in reference to an ECT sensor is 1 mm s^{-1}, and the sampling frequency of the ECT system is 37 frames per second. The unit in figure 9 is mm. The height of the reconstructed images is approximately the total length of an ECT sensor and the model in general, which means that the reconstructed images are stretched because of the existence of the axial length of an ECT sensor.

Figure 10(a) shows the motion of an object during the measurement, in which E is the effective length of the electrode in the sensor. We note that the motion could be divided into three stages according to the relative position of the object and electrodes. If we take the measurement of M1 by the ECT sensor L30 as an example, the measurement process can be correspondingly divided into three stages, as shown in figure 10. In the first stage (P1) the model gradually enters into the ECT sensor. The ratio of the volume of the model in the measurement area increases with the movement. In this stage, only part of the sensing region in the axial direction is occupied by the model. Therefore, the reconstructed images are stretched in the axial direction and contracted in the radial direction because of the uniform distribution, or the average effect of sensitivity in the axial direction, as shown in figure 8(a). Therefore, the reconstructed images of the cylinders turn into spindle shapes, and spheres are deformed and sharpened, which are less distorted than those of the cylinders. Such distortion happens in the entire stage of P1, which is even more serious for the ECT sensors with longer electrodes.

The second stage (P2) of the image means the model fully occupies the sensing region, and the image height in this stage is the absolute difference between the length of the electrodes and the model in the axial direction. Therefore, it can be classified into two categories according to the length difference between the ECT sensors and measured objects. If the length of the model is longer than an ECT sensor, the reconstructed 3D image would not be stretched in the axial direction, but remain averaged. In this case, the electrode length has less of an adverse effect on the reconstructed images than in P1, and no effect for a vertical-placed cylinder. If the length of the model is less than an ECT sensor, the reconstructed 3D image, compared with the real object, would still be stretched

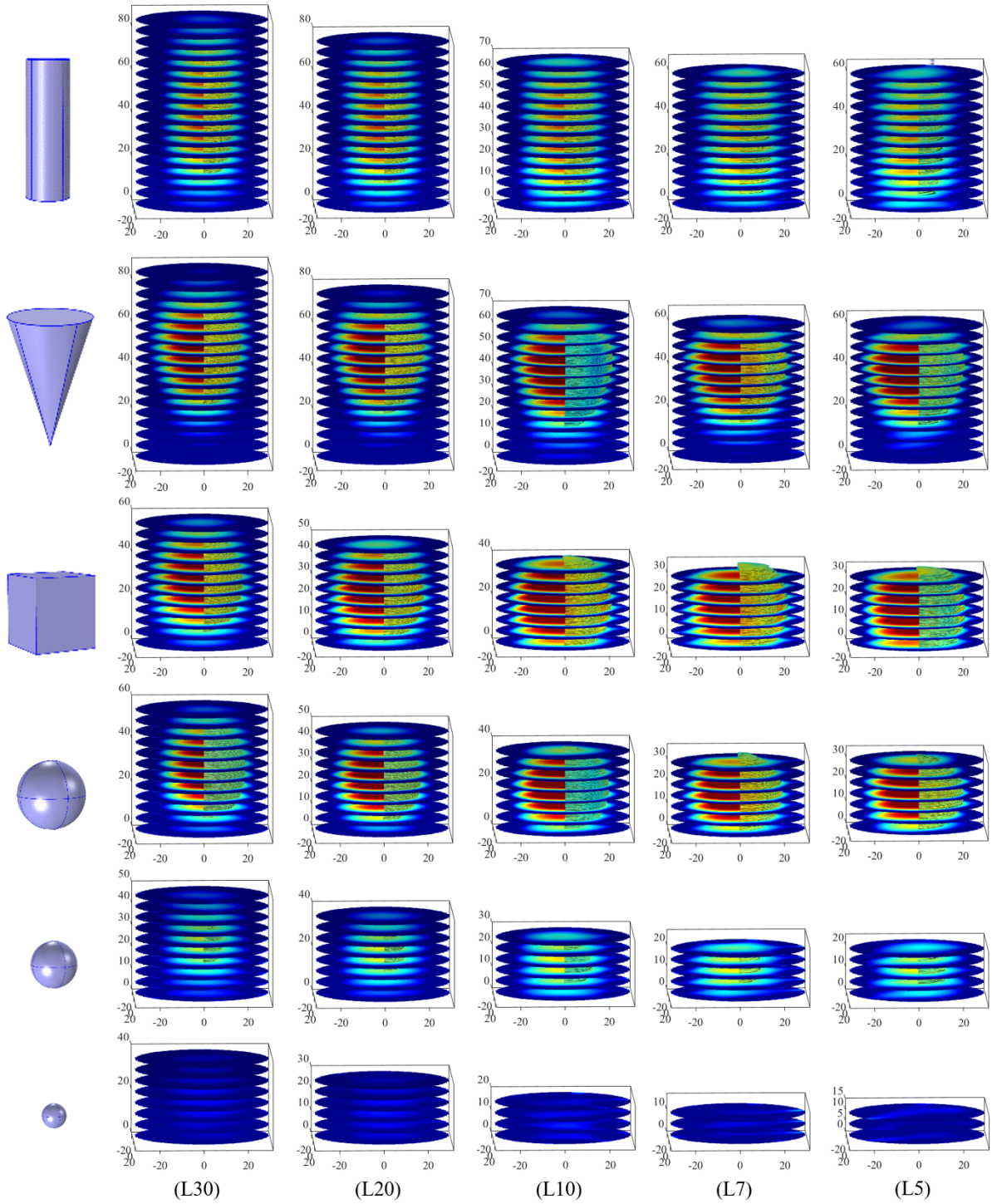

Figure 9. Reconstructed images of different models by ECT sensors with different electrode lengths when the movement velocity of the models is 1 mm s^{-1}.

in the axial direction, and the stretch length is the length difference between the ECT sensor and the model. Therefore, the length of an ECT sensor should be less than at least the length of the measured models to avoid serious axial average effects and image distortion in this stage. A sphere with a diameter of 20 mm can be well reconstructed by all the ECT sensors in figure 9; however, a sphere with a diameter of 10 mm cannot be recognized because the volume of the model, which is less than 1% of the entire sensing region, is too small to be measured. Therefore, the electrode length of an ECT sensor should not exceed 20 mm to achieve good performance from the perspective of image reconstruction.

The third stage (P3) of image reconstruction is the reserve process of P1, in which the model moves gradually out of the

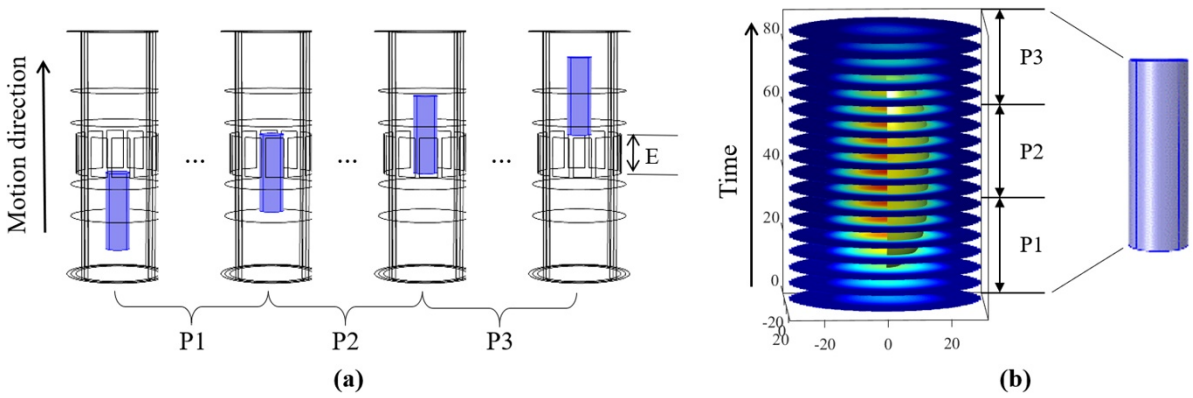

Figure 10. Derivation of 3D images using an ECT sensor with single-layer electrodes: (a) three stages of the motion of a phantom; (b) the corresponding three parts in the reconstructed 3D ECT image.

ECT sensor. The influence of electrode length on image reconstruction is similar to that at P1.

As can be seen, the electrode length of an ECT sensor has a serious impact on stages P1 and P3 in the processes of measurement and image reconstruction, in which severe distortion happens at the beginning of P1 and the end of P3. The longer the electrode length, the more serious the problem. The images only distort slightly for an object with permittivity distributed evenly along the axial direction in stage P2. To better image the structures of measured models, i.e. ensuring adequate measurement precision, the length of the electrodes in an ECT sensor should be as short as possible to decrease the axial average effect. In this case, however, the measured signals are weaker and more sensitive to the measurement errors. Moreover, there is no evident decrease in the fringe effect in the sensing region when the electrode length is below 10 mm [8, 35]. Therefore, it is not necessary to choose very short electrodes. Comprehensive analysis of the STD of the measured signals, the STD and CN of the sensitivity field and the quality of the reconstructed images shows that the ECT sensor L10 offers better measurement stability and accuracy.

As demonstrated above, the experiment results suggest that the intensity and stability of the measured signals of the ECT sensor L10 ares inferior to L20 and L30, but L10 has a larger CN of the sensitivity distribution than L20 and L30. But the relative velocity of the model regarding the ECT sensor was relatively low (1 mm s^{-1}). To verify the dynamic performance of L10, it is also necessary to test the objects moving with high velocity. Therefore, a higher relative velocity of the model regarding the ECT sensor, i.e. 10–300 mm s^{-1}, was also investigated. Typical reconstructed images for objects moving with a relative velocity of 10–300 mm s^{-1} using the ECT sensor L10 are shown in figure 11.

The moving velocities were 10, 100, 200 and 300 mm s^{-1}, respectively and the sampling frequency was about 37 frames/s. When the moving velocity is less than 100 mm s^{-1}, i.e. the movement distance in the time required for a frame of measurement data less than 3 mm, the velocity has little effect on the reconstructed images, because the movement distance is significantly shorter than the length of the reconstructed images in the axial direction. If the velocity exceeds 200 mm s^{-1}, it has obvious relative movement of the models in reference to the ECT sensor in a single frame of measurements, and the distortion caused by the motion of the reconstructed images becomes apparent. Whether or not the moving velocity of models and gas/solid phases in fluidized beds can be measured by ECT depends on the sampling rate of the sensing electronics.

4.4. Complicated objects

Above, we demonstrated the performance of the ECT sensor L10 with a single model object. We further studied the more complicated cases with the combination of multiple objects, including the combination of M1 and M5, and M4 and two M5. We obtained 3D images of these two combinations using the ECT sensor L10, and the results are shown in figure 12.

Then, we conducted experiments of the combinations of multiple objects, including the combination of M1 and M5 and the combination of M4 and two M5, with ECT sensor L10. The results are shown in figure 13. The image quality for 3D ECT images of both simple and multiple models has been quantitatively analyzed in terms of the image error (Ie) and the correlation coefficient (Cc) [10], as shown in table 1.

As can be seen, the quality of the reconstructed images of simple models is in general better than that of multiple models based on the 3D ECT experimental results, which is evidenced by the lower Ie and higher Cc for simple models. In particular, as observed in figure 13, it can be found that when two models are quite close, clear distortion exists in the reconstructed images, which is related to the intrinsic ill-conditioned and low spatial resolution of ECT since the shape edges are hard to identify. For multiple models, we compared the image quality of 3D ECT images obtained by experiments with that by simulations. As shown, the image quality by experiments is somehow worse than that by simulations. This may be due to the signal noise in the experiments being different from that in simulations.

The image quality could be improved to a certain extent if further image processing, such as filtering [28] and image segmentation [36], was implemented. In this work, we chose the fixed threshold image segmentation for the preliminary study.

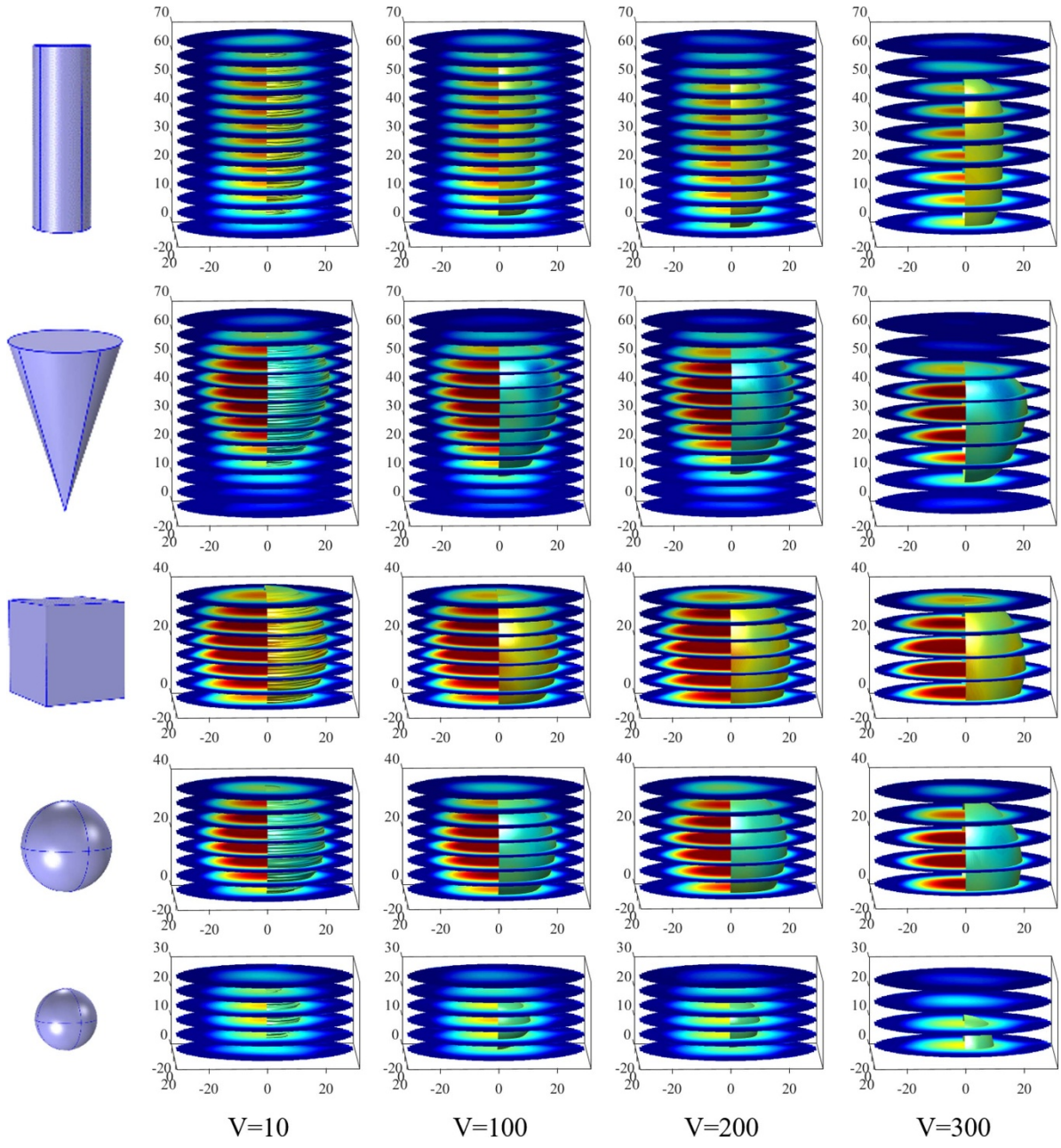

Figure 11. Reconstructed images of different models by the ECT sensor L10 with different relative velocities (mm s^{-1}).

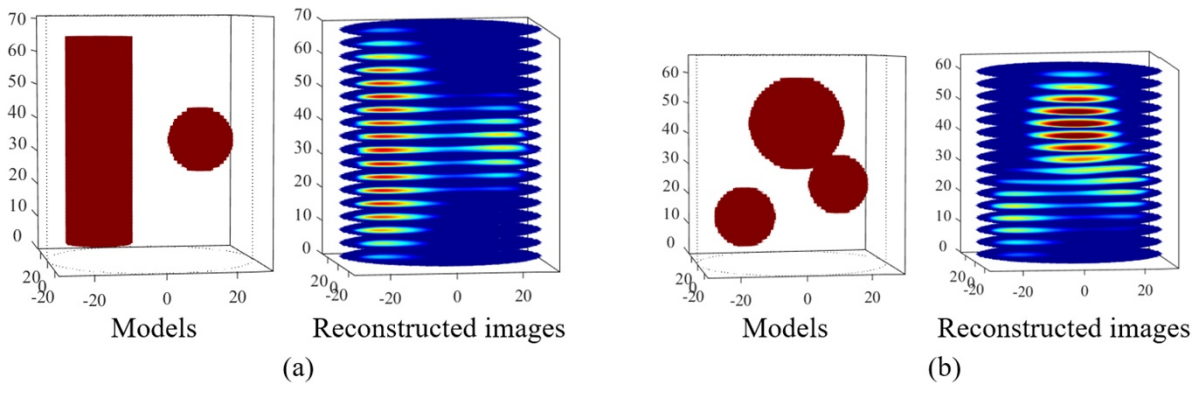

Figure 12. The reconstructed 3D images by the ECT sensor L10 by simulation: (a) the combination of M1 and M5, and (b) M4 and M5.

Table 1. The quantitative analysis of the image quality of different models with the ECT sensor L10: (1) without image processing, (2) with image processing.

		Experiment					Simulation	
		M1	M4	M5	Com1	Com2	Com1	Com2
(1)	Ie	0.75	0.88	0.96	0.77	0.94	0.59	0.58
	Cc	0.69	0.72	0.57	0.68	0.64	0.84	0.83
(2)	Ie	0.60	0.52	0.60	0.75	0.88	—	—
	Cc	0.80	0.87	0.79	0.68	0.67	—	—

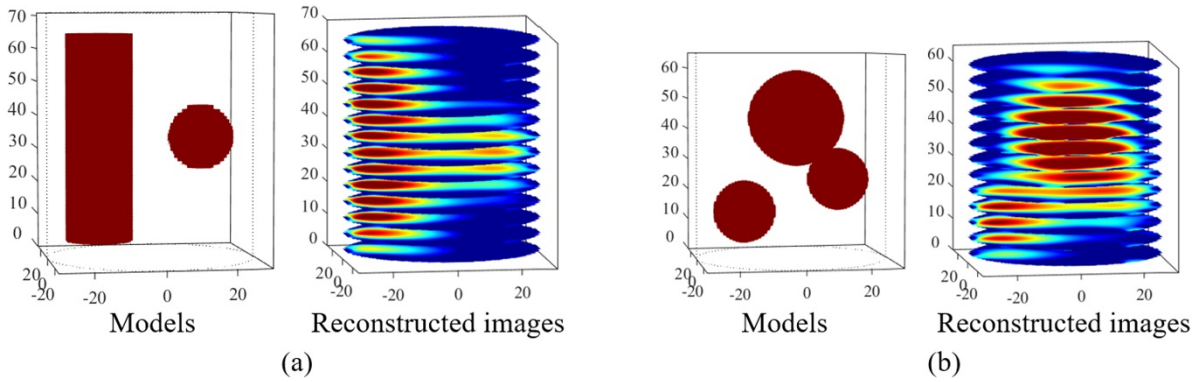

Figure 13. The reconstructed 3D images with ECT sensor L10 from experiments: (a) the combination of M1 and M5, and (b) M4 and M5.

A threshold of 0.8 was chosen for simple M4 and 0.6 for all other models, because M4 has a bigger volume in the sensing regions. Image processing is not conducted with the simulation data. After image processing, the quality of the images has been improved, especially for simple models in the sensing region. For the multiple models, both Ie and Cc show negligible improvement. It may be necessary to further optimize the threshold for complex models with different shapes and sizes. However, this is out of the scope of the current discussion as this work focuses on the effect of electrodes on 3D image reconstruction, although it deserves our research for the time being.

As can be seen, the ECT sensor L10 can successfully reconstruct the 3D images of the combination of M1 and M5 as well as the combination of M4 and two M5. We would stress, however, for ECT sensors with longer electrodes, the distortion of 3D images might become more severe owing to the lower spatial resolution. The quality of the reconstructed 3D ECT images for objects with complicated geometry depends heavily on the spatial resolution and suitable reconstruction algorithms and image processing. The effect of spatial resolution was discussed in section 4.2 from the viewpoint of sensitivity analysis. Note that it is our purpose in this paper to check the effect of the length of electrodes on the 3D ECT images; we are not going to address the influences of reconstruction algorithms and image processing in more detail. This, however, will be subject to our further work for the time being.

5. Conclusions

This paper compares the performance of ECT sensors with different electrode lengths, including the signal intensity, the precision of the measured signals, sensitivity distribution and the quality of reconstructed images. Comparison of the results of the ECT sensors with different electrode lengths shows that long electrodes are favorable to achieve the desired accuracy of the measured signals and CN of the sensitivity field. But the uniformly distributed sensitivity in the axial direction, or the axial average effect makes it difficult to reconstruct 3D images and causes serious distortion of the reconstructed images in the radial and axial directions. The reconstructed images of measured objects, which can be divided into three parts, are stretched in the axial direction and narrowed in the radial direction, and the total height of an image is about the sum of an ECT sensor and the measured objects. Because this effect was neglected in previous studies about the measurement of fluidized beds, the reconstructed images of bubbles or slugs have deformation or distortion. The ECT sensor L10 can reconstruct the 3D images of the measured models with relative realistic and reliable image quality under different test conditions. Comprehensive analysis of the performance of the ECT sensors in terms of the measured signals, sensitivity field and reconstructed images suggests that for an ECT sensor with electrodes mounted on the internal surface, the electrode length of 10 mm and dual-electrode excitation should be chosen.

Acknowledgments

The authors thank the National Key Research and Development Program of China (Grant No. 2018YFB0604904) for supporting this research.

ORCID iDs

Jingjing Shen https://orcid.org/0000-0002-1067-432X
Mao Ye https://orcid.org/0000-0002-7078-2402
Wuqiang Yang https://orcid.org/0000-0002-7201-1011

References

[1] Liu S, Fu L and Yang W Q 1999 Optimization of an iterative image reconstruction algorithm for electrical capacitance tomography *Meas. Sci. Technol.* **10** L37–L9
[2] Martin R, Ogarko V, Komatitsch D and Jessell M 2018 Parallel three-dimensional electrical capacitance data imaging using a nonlinear inversion algorithm and L-p norm-based model regularization *Measurement* **128** 428–45
[3] Deabes W, Sheta A, Bouazza K E and Abdelrahman M 2019 Application of electrical capacitance tomography for imaging conductive materials in industrial processes *J. Sens.* **2019** 4208349
[4] Chandrasekera T C, Li Y, Moody D, Schnellmann M A, Dennis J S and Holland D J 2015 Measurement of bubble sizes in fluidised beds using electrical capacitance tomography *Chem. Eng. Sci.* **126** 679–87
[5] Huang K, Meng S, Guo Q, Ye M, Shen J, Zhang T, Yang W and Liu Z 2018 High-temperature electrical capacitance tomography for gas-solid fluidised beds *Meas. Sci. Technol.* **29** 104002
[6] Li X, Jaworski A J and Mao X 2018 Bubble size and bubble rise velocity estimation by means of electrical capacitance tomography within gas-solids fluidized beds *Measurement* **117** 226–40
[7] Soleimani M, Wang H, Li Y and Yang W 2007 A comparative study of 3D electrical capacitance tomography *Int. J. Inf. Sys. Sci.* **3** 292–306
[8] Yang W Q 2010 Design of electrical capacitance tomography sensors *Meas. Sci. Technol.* **21** 042001
[9] Li Y and Holland D J 2013 Fast and robust 3D electrical capacitance tomography *Meas. Sci. Technol.* **24** 105406
[10] Ye J, Wang H and Yang W 2016 Characterization of a multi-plane electrical capacitance tomography sensor with different numbers of electrodes *Meas. Sci. Technol.* **27** 035103
[11] Li Y and Holland D J 2015 Optimizing the geometry of three-dimensional electrical capacitance tomography sensors *IEEE Sens. J.* **15** 1567–74
[12] Ye J, Mao M, Wang H and Yang W 2015 An evaluation of the rotation of electrodes in multi-plane electrical capacitance tomography sensors *Meas. Sci. Technol.* **26** 125404
[13] Warsito W and Fan L S 2003 3D-ECT velocimetry for flow structure quantification of gas-liquid-solid fluidized beds *Can. J. Chem. Eng.* **81** 875–84
[14] Qiu G Z, Ye J M, Wang H G and Yang W Q 2014 Investigation of flow hydrodynamics and regime transition in a gas-solids fluidized bed with different riser diameters *Chem. Eng. Sci.* **116** 195–207
[15] Ge R H, Ye J M, Wang H G and Yang W Q 2016 Investigation of gas-solids flow characteristics in a conical fluidized bed dryer by pressure fluctuation and electrical capacitance tomography *Drying Technol.* **34** 1359–72
[16] Che H Q, Ye J M, Tu Q Y, Yang W Q and Wang H G 2018 Investigation of coating process in Wurster fluidised bed using electrical capacitance tomography *Chem. Eng. Res. Des.* **132** 1180–92
[17] Liu S, Chen Q, Wang H G, Jiang F, Ismail I and Yang W Q 2005 Electrical capacitance tomography for gas-solids flow measurement for circulating fluidized beds *Flow Meas. Instrum.* **16** 135–44
[18] Huang K, Meng S H, Guo Q, Yang W Q, Zhang T, Ye M and Liu Z M 2019 Effect of electrode length of an electrical capacitance tomography sensor on gas-solid fluidized bed measurements *Ind. Eng. Chem. Res.* **58** 21827–41
[19] Warsito W and Fan L S 2005 Dynamics of spiral bubble plume motion in the entrance region of bubble columns and three-phase fluidized beds using 3D ECT *Chem. Eng. Sci.* **60** 6073–84
[20] Yang W Q and Conway W F 1998 Measurement of sensitivity distributions of capacitance tomography sensors *Rev. Sci. Instrum.* **69** 233–6
[21] Weber J M, Bobek M M, Breault R W, Mei J S and Shadle L J 2018 Investigation of core-annular flow in an industrial scale circulating fluidized bed riser with electrical capacitance volume tomography (ECVT) *Powder Technol.* **327** 524–35
[22] Cui Z, Wang Q, Xue Q, Fan W, Zhang L, Cao Z, Sun B, Wang H and Yang W 2016 A review on image reconstruction algorithms for electrical capacitance/resistance tomography *Sens. Rev.* **36** 429–45
[23] Yang W Q 1996 Hardware design of electrical capacitance tomography systems *Meas. Sci. Technol.* **7** 225–32
[24] Gu L, Zhang Y and Zhu J 2020 Wavelet denoising and nonlinear analysis of solids concentration signal in circulating fluidized bed riser *Particuology* **49** 105–16
[25] Yang W Q and York T A 1999 New AC-based capacitance tomography system *IEE Proc. Sci. Meas. Technol.* **146** 47–53
[26] Yang W Q 2001 Further developments in an ac-based capacitance tomography system *Rev. Sci. Instrum.* **72** 3902–7
[27] Yang W Q and Peng L H 2003 Image reconstruction algorithms for electrical capacitance tomography *Meas. Sci. Technol.* **14** R1–R13
[28] Xie C G, Huang S M, Hoyle B S, Thorn R, Lenn C, Snowden D and Beck M S 1992 Electrical capacitance tomography for flow imaging: system model for development of image reconstruction algorithms and design of primary sensors *IEE Proc. G Circuits Devices Sys.* **139** 89–98
[29] Peng L H, Merkus H and Scarlett B 2000 Using regularization methods for image reconstruction of electrical capacitance tomography *Part. Part. Sys. Charact.* **17** 96–104
[30] Yang W Q, Spink D M, York T A and McCann H 1999 An image-reconstruction algorithm based on Landweber's iteration method for electrical-capacitance tomography *Meas. Sci. Technol.* **10** 1065–9
[31] Marashdeh Q, Warsito W, Fan L S and Teixeira F L 2006 A nonlinear image reconstruction technique for ECT using a combined neural network approach *Meas. Sci. Technol.* **17** 2097–103
[32] Clark P J, Forte G, Simmons M J H and Stitt E H 2016 Towards 3D-electrical capacitance tomography for interface detection thresholding method improves accuracy for real-world 3D process monitoring *Johnson Matthey Technol. Rev.* **60** 164–75
[33] Andryani N A C, Sudiana D and Gunawan D 2018 Compressive sensing approach with double layer soft threshold for ECVT static imaging *5th Int. Conf. Information Technology, Computer, and Electrical Engineering* pp 379–84
[34] Dyakowski T, Edwards R B, Xie C G and Williams R A 1997 Application of capacitance tomography to gas-solid flows *Chem. Eng. Sci.* **52** 2099–110
[35] Hammer E A and Green R G 1983 The spatial filtering effect of capacitance transducer electrodes (flow measurement) *J. Phys. E: Sci. Instrum.* **16** 438–43
[36] Agrawal V, Shinde Y H, Shah M T, Utikar R P, Pareek V K and Joshi J B 2018 Estimation of bubble properties in bubbling fluidized bed using ECVT measurements *Ind. Eng. Chem. Res.* **57** 8319–33